6.8 Application

The ideal power, heat input and heat rejected are respectively modified by the losses as follows:

$$P_a = P_i - \sum_{k,r,h}\langle\Phi\rangle_j - \sum_{d,b}\langle\dot{W}\rangle_{gsj} - \sum_{c,e}\langle\dot{W}\rangle_{gj} - \sum_{d,p,gs}\langle\Phi\rangle_{\ell j} - (-\langle\dot{H}_L\rangle_{gas} - \langle\dot{W}\rangle_{seal})$$
$$- \sum_{d,p,gs}\langle\dot{W}\rangle_{sj} \tag{6.97}$$

$$\langle\dot{Q}_h\rangle_a = \langle\dot{Q}_h\rangle_i - \langle\Phi\rangle_h - \tfrac{1}{2}\langle\Phi\rangle_r + \langle\dot{Q}_r\rangle_i(1-\epsilon) + \sum_{j=1}^{n}\dot{Q}_{cj} - \langle\dot{W}\rangle_{ge}$$
$$- (-\langle\dot{H}_{sh}\rangle) \tag{6.98}$$

$$\langle\dot{Q}_k\rangle_a = \langle\dot{Q}_k\rangle_i - \langle\Phi\rangle_k - \tfrac{1}{2}\langle\Phi\rangle_r - \langle\dot{Q}_r\rangle_i(1-\epsilon) - \sum_{j=1}^{n}\dot{Q}_{cj} - \langle\dot{W}\rangle_{gc} - \sum_{d,p,gs}\langle\Phi\rangle_{\ell j}$$
$$- \left[(-\langle\dot{H}_{sh}\rangle) + (-\langle\dot{H}_L\rangle_{gas}) - \langle\dot{W}\rangle_{seal}\right] - \sum_{d,p,gs}\langle\dot{W}\rangle_{sj} \tag{6.99}$$

where the subscripts indicate the following:

- a : actual
- b : bounce space
- c : compression space
- cj : j'th conduction path
- d : displacer
- e : expansion space
- gc : compression space hysteresis
- ge : expansion space hysteresis
- gs : gas spring
- h : heater
- i : ideal
- j : index
- k : cooler
- ℓj : j'th leakage path
- p : piston
- r : regenerator
- sj : j'th ring seal

(6.99) may be slightly simplified by collecting the terms that make up the appendix loss.

$$\langle \dot{Q}_k \rangle_a = \langle \dot{Q}_k \rangle_i - \langle \Phi \rangle_k - \tfrac{1}{2}\langle \Phi \rangle_r - \langle \dot{Q}_r \rangle_i (1 - \epsilon) - \sum_{j=1}^{n} \dot{Q}_{cj} - \langle \dot{W} \rangle_{gc} - \sum_{d,p,gs} \langle \Phi \rangle_{\ell j}$$
$$- \langle \dot{Q}_a \rangle - \sum_{d,p,gs} \langle \dot{W} \rangle_{sj} \tag{6.100}$$

The ideal quantities would preferably be obtained from the ideal adiabatic or pseudo Stirling cycle (Appendix C), though the Schmidt analysis seems to work quite well for machines of low compression ratio. Obviously in the case of the adiabatic analysis the power is reduced by the adiabatic loss whereas in the Schmidt analysis it is not. Since wall/gas ΔT irreversibilities are not included in the above equations, the ideal quantities are based on the bulk gas cooler and heater temperatures. Given the heat transfer, the temperature drop from gas to wall is calculated from the heat transfer coefficient as outlined in §4. Depending on heat exchanger loading, the gas temperatures will vary and thus change the ideal power.

Note once again that the reduction of power due to dissipating effects occurs mainly by reducing the pressure phase angle with respect to the piston.

Table 6.1 lists loss inventories for the three example engines contained in Appendix A. Since the losses are difficult to measure individually, comparisons are based on the overall performance figures (Table 6.2). No systematic error analysis for the RE-1000 or GPU-3 engines seem to be available. The GPU-3 data comes from a single steady state point, the RE-1000 data is representative of a larger set of data, one test point of which was done at Sunpower, the rest being done at NASA-Lewis. Figures 6.19 and 6.20 are typical performance curves from the NASA data [Sc83.2]. Most position and pressure (or force) transducers are fairly accurate (less than 1% error), the usual source of error is in measuring the phase angle between the pressure (or force) and position in order to calculate power (Equation 6.45). Sunpower's experience is that the error on smaller phase angle measurements (around 20°) is in the neighbourhood of 5% or slightly larger. The error in power would therefore be around 5%. Efficiency is generally more difficult to measure. The usual practice is to measure the cooling water flow rate and entrance and exit temperatures from which the heat removed at the cooler is calculated with good accuracy. The heat into the engine is then assumed to be the indicated work plus the heat removed at the cooler, the indicated efficiency is then based on this calculation. Obviously, calculating efficiency in this way does not account for heat leaving the engine from sources other than the cooler. This approach should not lead to large errors provided that the heat leaving the engine's other surfaces is by free convection. The degree of this error has not been estimated. In the case of the RE-1000, the engine is well insulated from the ambient and the heat input is done by electrically heating the heater tubes (see Figure A.4), the heat input is thus well defined by measuring voltage and current and the error here would be less than 5%. For the other engines it must be assumed that the efficiency measurements are slightly optimistic.

Table 6.1 Calculated Loss Inventories

	GPU-3	RE-1000	SPIKE.S	SPIKE.D
Viscous dissipation [W]:				
Cooler	101	22	147	182
Regenerator	938	38	290	358
Heater	162	42	10	33
Gas hysteresis [W]:				
Compression space	31	7	11	10
Expansion space	83	17	27	20
Gas spring	0	8	101	109
Bounce space	56	small	25	33
Seal leakage [W]:				
Displacer	?	small	small	small
Piston	?	74	small	small
Gas spring puck	-	-	-	63
Rod (at displacer)	-	30	31	small
Rod (at piston)	?	0	28	142
Conduction [W]:				
Gas	94	25	112	81
Regenerator walls	987	178	290	207
Internal walls	686	69	148	113
Seal friction [W]:				
Displacer	0	24	small	small
Piston	0	small	147	158
Rod (at displacer)	0	small	small	small
Rod (at piston)	0	-	small	small
Gas spring	0	-	-	small
Appendix loss [W]:				
Gas enthalpy	524	123	168	142
Shuttle	676	79	29	44
Regenerator enthalpy loss [W]	1620	680	523	909
Temperature differentials [K]:				
Cooler	24.2	6.3	8.6	11.9
Heater	33.9	20.9	88.3	30.6

Table 6.2 Comparison with Experimental Results

	GPU-3 [1]	RE-1000 [2]	SPIKE.S [3]	SPIKE.D [3]
Operating parameters:				
Hot wall temperature [K]	977	873	846	710
Cold wall temperature [K]	288	303	297	320
Charge pressure [bar] (abs)	41.3	71	11	12
Frequency [Hz] (crank type)	41.72	-	-	-
Piston amplitude [mm]	13.8	13.1	14.0	14.4
Displ. ampl. [mm] (crank)	15.6∠65°	-	-	-
Experimental performance parameters:				
Engine power [kW]	3.96	1.2	1.57	1.25
Engine efficiency [%]	35	29	26	18-20
Experimental free-piston dynamic parameters:				
Frequency [Hz]	-	30.2	60.0	61.9
Stroke ratio	-	1.1	0.72	0.97
Displacer/piston phase [°]	-	47.6	65.7	57.5
Calculated performance:				
Engine power [kW]	4.79	1.4	1.29	1.27
pV power [kW]	4.85	1.4	1.46	1.46
Engine efficiency [%]	37	35.4	24.7	18.4
pV efficiency [%]	37.3	35.4	28.1	21.2
Calculated free-piston dynamic parameters:				
Frequency		30.3	59.2	60.4
Stroke ratio		0.87	0.76	0.99
Displacer/piston phase [°]		59.2	59.9	56.7

1) Data from [Th79]

2) Data from [Sc83.1, Sc83.2]

3) Data from Sunpower files

In practice, the performance of a particular engine varies significantly with extraneous issues, eg, dirt in the engine or significant wear on one of the parts allowing greater leakage to occur, etc. Where possible, therefore, the data chosen are taken from significant steady state runs, ie, where the engine's performance remains steady for in excess of an hour.

From Table 6.2, the largest discrepancy between experiment and calculation is for the GPU-3 engine. This engine has the highest compression ratio of the engines presented here and the motions of the moving parts are non-sinusoidal. Therefore errors associated with linearization are likely to be higher. Furthermore, losses associated with leakage and friction could not be estimated since detailed information of the seals was not available. These dissipating losses could have a significant effect on the calculated power. Tew *et al* [TJ78] did include a leakage loss in their simulation calculations of the GPU-3 and found it to greatly change the time taken for convergence even at a net loss of only 79W. However, the leakage factor used was arbitrary and may not be indicative of the leakage losses in this machine. Displacer friction losses would certainly be significant since they would increase the amount of energy fed back to the cycle by the mechanism.

The discrepancy in the single acting gas spring SPIKE seems to suggest a higher displacer resonance than that calculated (phase angle calculates low). From Figure 5.17 it can be seen that the displacer was indeed not centering properly, ie, it was oscillating at a point lower down on the rod thus reducing its gas spring volume and so increasing its resonance.

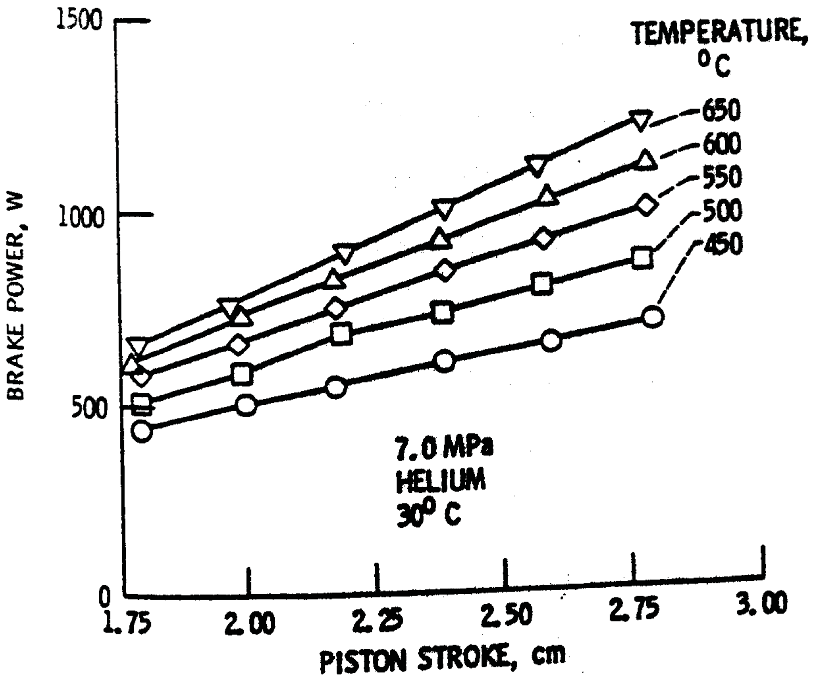

Figure 6.19 Power versus Piston Stroke for RE-1000 [Sc83.2]

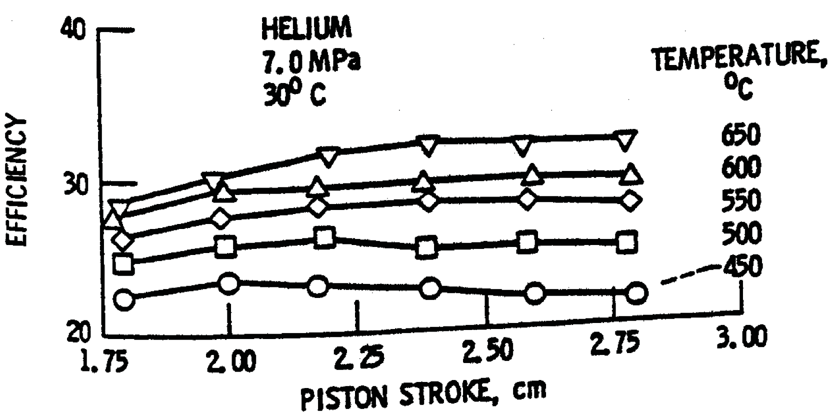

Figure 6.20 Efficiency versus Stroke for RE-1000 [Sc83.2]

As may be expected, closest correlation occurs for the more linear double acting gas spring SPIKE engine. The non-linearities for the GPU-3 and the single acting gas spring SPIKE are more severe than the RE-1000 and the double acting spring SPIKE, and therefore correlation may be expected to be poorer for these engines. However, for the three widely differing engines analysed here, it can be seen that the simple linear type analysis and discrete loss calculations can return realistic results. The important aspect of this type of analysis is to indicate the structure of the various processes in the cycle so that the relative magnitudes of these processes may be judged. Great accuracy is thus not necessarily required, though in the examples treated here, the linear analysis has predicted the performance of some of the sample engines with good accuracy. Figure 6.21 is a computer simulation of the RE-1000 (also taken from [SC83.1]), showing power as a function of hot end temperature and piston stroke. This simulation appears to have been done with fixed dynamics since the power growth with stroke seems to be linear. In a free dynamics simulation it would be expected that the displacer amplitude would also grow with piston amplitude thus the power growth with piston stroke should be approximately second order (see S3). Nevertheless, comparing the simple analysis (Table 6.2) with Figure 6.21 the agreement can be seen, in this case, to be reasonably close with a typical third order calculation.

Table 6.3 lists the pertinent equations derived in this section.

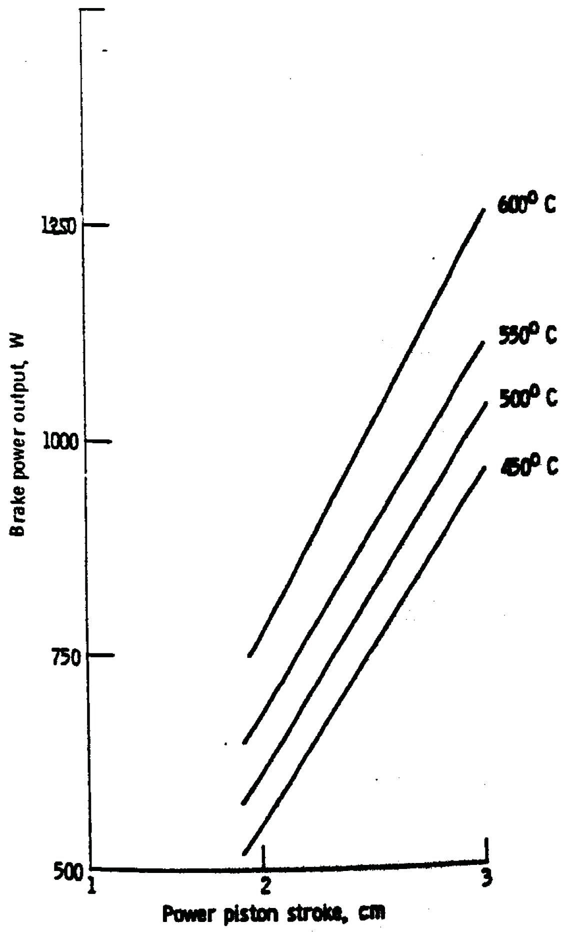

Figure 6.21 Simulation Power versus Piston Stroke for RE-1000 [Sc83.1]

Table 6.3 Parasitic Losses Summary

Conduction

$$\dot{Q} = Ak(\Delta T/\Delta x)$$

Gas Hysteresis

Gas spring

$$\langle \dot{W} \rangle_{gs} \approx \sqrt{(1/32)\omega\gamma^3(\gamma - 1)T_w \langle p \rangle k}\,(\Delta V/V_d)^2 A_w$$

or

$$\langle \dot{W} \rangle_{gs} \approx (k/4)\sqrt{\omega/(2\bar{\alpha})}\,\gamma(\gamma - 1)T_w A_w (\Delta V/V_d)^2$$

Working spaces

$$\langle \dot{W} \rangle_g = \sqrt{(\omega/32)\bar{\alpha}}\,A_w |p|^2/(\gamma \langle p \rangle)$$

Clearance seal leakage

Leakage dissipation

$$\langle \Phi \rangle_L = \pi D \left\{ (L\,\mu/c)|U_p|^2/2 + c^3/(24\mu L)\left[|p_a|^2 - 2|p_a||p_b|\cos(\phi_a - \phi_b) + |p_b|^2\right]\right\}$$

Zero leakage length

$$L_0 = (1/6)\left[2(\langle p_b \rangle^2 - \langle p_a \rangle^2) - |p_a|^2\right]c^2/(\mu |U_p||p_a|\sin\phi_a)$$

Effective clearance

$$\bar{c} = (1 + e^2)^{1/3}c$$

Table 6.3 Parasitic Losses Summary - Continued

Appendix Gap

Shuttle (general)

$$\langle \dot{H}_{sh} \rangle = -(\pi/2) D k X_d^2 (T_h - T_\ell)/(L h)$$

Shuttle (limiting value)

$$\langle \dot{H}_{sh} \rangle_{lim} = -(\pi/4) D k X_d^2 \sqrt{\omega/(2\bar{\alpha}_h)}\,(T_h - T_\ell)/L$$

Gas enthalpy transport

$$\langle \dot{H}_L \rangle_{gas} = -c_p \omega \langle m_a \rangle r (X_d/L)(T_h - T_\ell)\left[1/2 - k/(k_s w h)\right](1/\pi - \cos\phi_m/4)$$

where $r = \left[(r_p \cos\phi + r_T - r_x)^2 + (r_p \sin\phi)^2\right]^{1/2}$ and

$$\phi_m = \tan^{-1}\left[(r_p \cos\phi + r_T - r_x)/(r_p \sin\phi)\right]$$

Seal work

$$\langle \dot{W} \rangle_{seal} = -\tfrac{1}{2}\pi D |p| h X_d \omega \sin\phi$$

Energy balance

$$\langle \dot{Q}_a \rangle = (-\langle \dot{H}_{sh} \rangle) + (-\langle \dot{H}_L \rangle_{gas}) - \langle \dot{W} \rangle_{seal}$$

Table 6.3 Parasitic Losses Summary – Continued

Mechanical Friction

$$W_s = \mu A_s X\left[\left|(|p_a|\cos\phi_a - |p_b|\cos\phi_b)\right| + (\pi/2)\left|(|p_a|\sin\phi_a - |p_b|\sin\phi_b)\right|\right] + 4F_{sc}X$$

Energy Balance

Output power

$$P_a = P_i - \sum_{k,r,h}\langle\Phi\rangle_j - \sum_{d,b}\langle\dot{W}\rangle_{gsj} - \sum_{c,e}\langle\dot{W}\rangle_{gj} - \sum_{d,p,gs}\langle\Phi\rangle_{Lj} - (-\langle\dot{H}_L\rangle_{gas} - \langle\dot{W}\rangle_{seal}) - \sum_{d,p,gs}\langle\dot{W}\rangle_{sj}$$

Heat in

$$\langle\dot{Q}_h\rangle_a = \langle\dot{Q}_h\rangle_i - \langle\Phi\rangle_h - \tfrac{1}{2}\langle\Phi\rangle_r + \langle\dot{Q}_r\rangle_i(1-\epsilon) + \sum_{j=1}^{n}\dot{Q}_{cj} - \langle\dot{W}\rangle_{ge} - (-\langle\dot{H}_{sh}\rangle)$$

Heat out

$$\langle\dot{Q}_k\rangle_a = \langle\dot{Q}_k\rangle_i - \langle\Phi\rangle_k - \tfrac{1}{2}\langle\Phi\rangle_r - \langle\dot{Q}_r\rangle_i(1-\epsilon) - \sum_{j=1}^{n}\dot{Q}_{cj} - \langle\dot{W}\rangle_{gc} - \sum_{d,p,gs}\langle\Phi\rangle_{Lj} - \langle\dot{Q}_d\rangle - \sum_{d,p,gs}\langle\dot{W}\rangle_{sj}$$

where the subscripts indicate the following:

- a: actual
- b: bounce space
- c: compression space
- cj: j'th conduction path
- d: displacer
- e: expansion space
- gc: compression space hysteresis
- ge: expansion space hysteresis
- gs: gas spring
- h: heater
- i: ideal
- j: index
- k: cooler
- Lj: j'th leakage path
- p: piston
- r: regenerator
- sj: j'th ring seal

7 A DESIGN PROCEDURE

7.1 Operating Temperatures

For maximum available efficiency the gas temperature ratio (T_h/ T_k) must be maximized. All else being equal, maximum temperature ratio also gives the greatest work output for a given size engine. Optimum efficiency is, however, not always appropriate. Particularly where the trade off between engine base cost and operating cost favours a lower base cost which would generally compromise the efficiency and so increase the operating cost [Be84].

The cold end temperature is usually close to the sink temperature which, in most cases, is the ambient temperature. An example where this is not the case is in cogeneration, where the rejected heat may be used to raise steam or produce hot water. Where heat is supplied by combustion or solar radiation the hot end temperature is more typically a design variable since the maximum hot temperature is limited mainly by materials and, to some degree, geometry. In this section, the effect of geometry and material selection on the maximum hot end temperature will be briefly discussed.

Heaters in Stirling engines are generally either constructed from a multiple of finned tubes or a monocoque finned head. Heat may be supplied directly by combustion gases or indirectly by way of heat pipes. Tubular heat exchangers involve many small components which must be assembled and brazed with gas tight integrity. Such heat exchangers tend to be expensive compared to a cast head with integral fins (monocoque type). High pressure engines (50bar and above) are of small diameter thus making it difficult to configure integral external heat exchangers in the available space. Higher heat fluxes on integrally finned heads make it necessary to use a combination of larger combustion blowers and higher surface temperatures in order to transmit the required heat. Both these requirements lead to an expensive construction often requiring super alloy components. The advantage of the tubular heat exchanger is that its vastly superior surface area allows much smaller blower powers and lower peak temperatures to be used. Also, since the pressure stresses are proportional to diameter, the small diameter tubes are able to be much thinner, thus reducing the temperature drop across the wall. An example of a tubular heat exchanger is shown in Appendix A, Figure A.5. This 2.5kW RE-1000 derivative required only 10W to the combustion blower and the highest temperature on the fins was 700°C. The low power blower is also very quiet which is often a further advantage.

However, the problem of expense associated with the complexity of the tubular heat exchanger is always a concern, particularly in engines of lower power where the cost of the head tends to be a larger fraction of the system cost.

Since the strength of the heater head material drops off sharply with temperature; the higher the temperature, the thicker the wall needs to be to contain a fixed pressure. The conduction temperature drop across the wall also increases with wall thickness, thus there is a finite upper temperature which maximizes the internal wall temperature. A simple calculation illustrates this effect.

Neglecting bending due to end conditions, the major stress is the hoop stress given by

$$\sigma_h = pD/(2t)$$

where D is diameter and t is thickness.

For a given allowable stress, the wall thickness is then

$$t = pD/(2\sigma_h) \tag{7.1}$$

From Fourier's conduction law, the temperature gradient across the wall is given by

$$\Delta T / t = \dot{q}/k \tag{7.2}$$

where $\dot{q}$ is the heat flux [W/m²K].

Thus from (7.1) and (7.2) the internal wall temperature is

$$T_h = T_s - \dot{q}pD/(2\sigma_h k) \tag{7.3}$$

Both σ_h and k are functions of temperature. Figures 7.1 (a) and (b) show the effect of temperature on the rupture strength and thermal conductivity of 300 series stainless steel. Using 347 type stainless steel, Equation 7.3

is plotted in Figure 7.2 for engine parameters similar to the SPIKE engine in Appendix A.3 and for a larger 4kW engine. Both engines are assumed to have integrally finned heater heads with the following engine parameters:

SPIKE: $\langle p \rangle = 12\text{bar}$, $\dot{q} \approx 122\text{kW/m}^2$, $D = 174\text{mm}$

4kW: $\langle p \rangle = 24\text{bar}$, $\dot{q} \approx 400\text{kW/m}^2$, $D = 231\text{mm}$.

From Figure 7.2 it is clear that for this type of material and head design, the 4kW engine's hot end temperature is strongly compromised by the temperature drop across the wall. For higher powers the temperature drop will be greater which will reduce the internal wall temperature to below 700°C. On the other hand, the 1kW engine's hot internal wall temperature is limited by corrosion considerations on the external wall. From a strength point of view, the 1kW heater head may be designed for temperatures exceeding 700°C and may be of the integrally finned type. In order to use an integrally finned head on the higher power engine it would be necessary to either find a material of significantly greater high temperature strength or reduce the heat flux. Reducing the heat flux at constant power (P) would require a larger area for heat transfer. Since $P \propto D^2 \langle p \rangle$ and the heat transfer area is proportional to diameter, reducing the heat flux would produce a larger diameter lower pressure engine which would be of lower specific power. Higher power engines (greater than 4kW) would generally use tubular heat exchangers, though with super alloys and the newer ceramic materials it should be possible to extend the practicality of integrally finned heads. In reality, the effect of wall temperature drop will be even stronger than indicated here since the efficiency will drop with falling hot end temperature thus requiring higher heat fluxes for the same power.

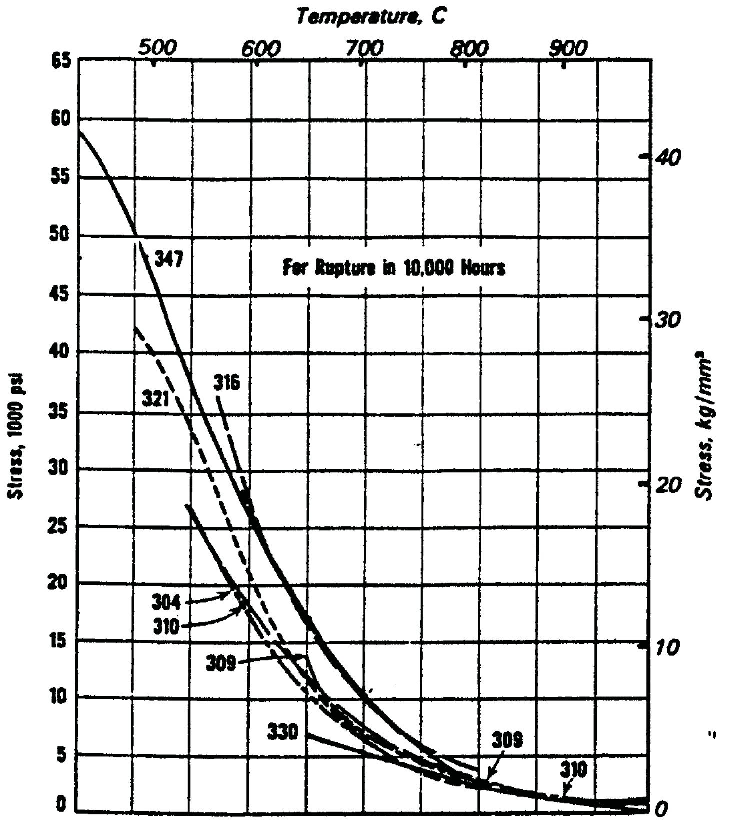

Figure 7.1(a) Stress-Rupture Curves for Several 300 Series Stainless Steels [INL66]. To obtain stress in Pa, multiply by 6895.

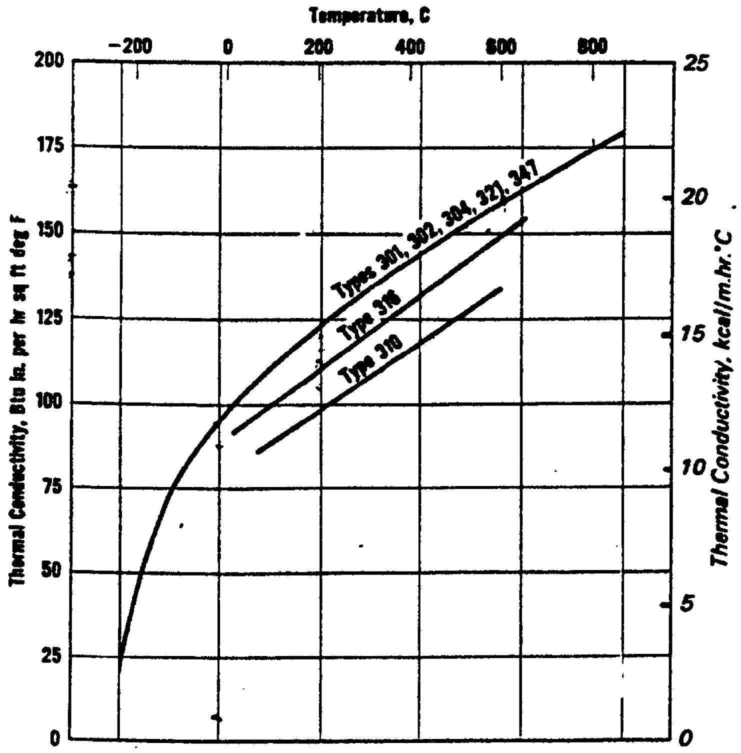

Figure 7.1(b) Effect of Temperature on Thermal Conductivity of Several 300 Series Stainless Steels [INL66]. To obtain thermal conductivity in W/mK, multiply by 0.1444.

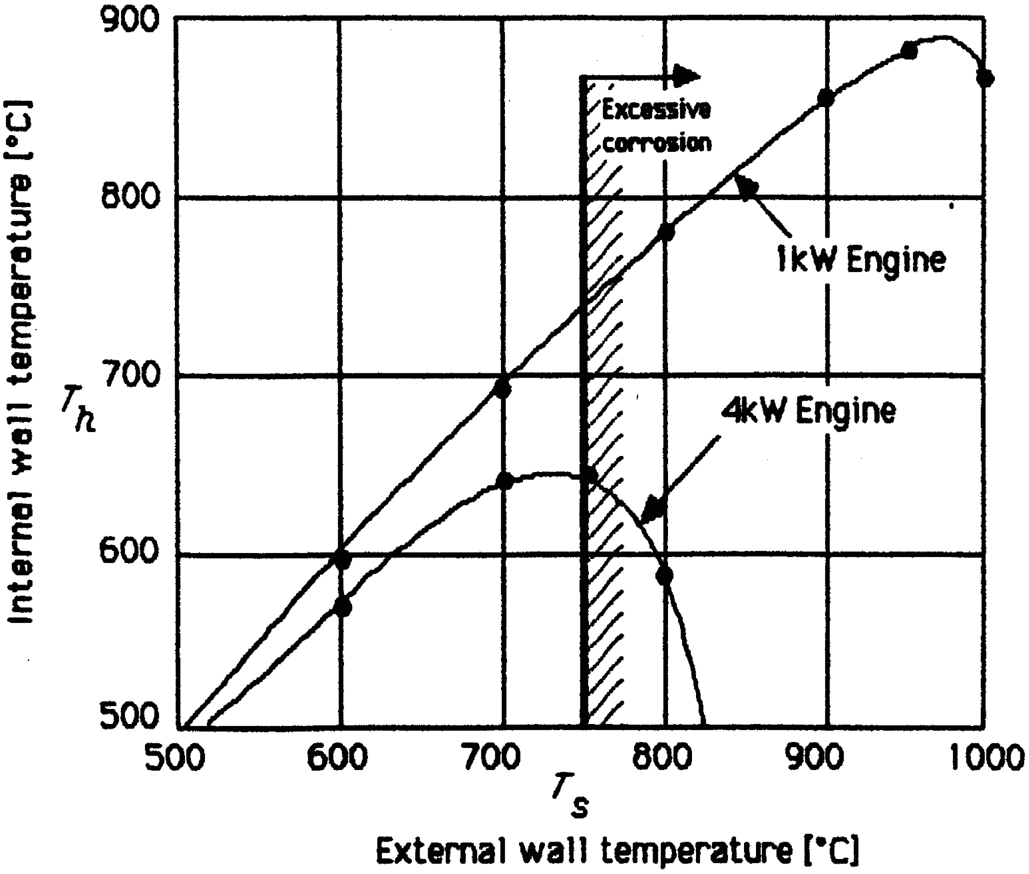

Figure 7.2 Internal Wall Temperature versus External Wall Temperature for Integrally Finned Heads

Convective heat transfer surface area is also limited at the larger power levels for integrally finned heads. Therefore, in order to transfer the required heat, the heat transfer coefficient is increased by increasing the combustion gas velocity. This leads to higher blower powers which reduce the system efficiency. Similar disadvantages apply to the internal convective heat transfer, but generally to a lower degree than the external convective heat transfer.

In the SPIKE engine the integrally finned head requires only 10W of blower power, however, the engine has a fairly large diameter to obtain a low heat flux and the charge pressure is only 12bar (maximum). Even so, the engine/alternator package is compact as can be seen in Figure A.9 (Appendix A) and has a mass of 30kg.

The details of the above arguments would be modified by the use of some novel heat exchangers. For example, heat pipes have been proposed by Meijer and Ziph [MZ82], Dunn *et al* [DR82] and Musikant *et al* [MC85] which would, to a large degree, remove the exterior convective heat transfer restriction. Heat pipe configurations vary, but one possibility is to pass the heat pipe through the pressure vessel wall so that the condenser is in the expansion space. The heat transfer wall is then across the relatively small diameter of the heat pipe.

7.2 Selection of Working Gas

The following is partially taken from [BR85]. Discussion on the practical merits of various working gases is not entered into since it is felt that these considerations are generally either obvious or dictated by the application at hand. The impact of working gas on the choice of materials insofar as corrosion, embrittlement and gas permiation is concerned is beyond the scope of this work.

To give a preliminary idea of the comparison between various working gases consider that in order to obtain similar performance between engines of similar power using different working gases, the total engine irreversibilities should also be similar. Irreversibilities are functions of temperature gradients and viscous dissipation (Appendix B). Therefore an equivalent statement of similar performance would be: for given operating temperatures; if the temperature gradients and viscous dissipation is similar in engines with different working gases and similar powers, then the overall performances should also be similar.

Temperature change in the direction of flow in the heat exchangers is given by

$$\dot{Q} = w\, c_p\, \Delta T \tag{7.4}$$

from §3.8, the mass flow is proportional as follows

$$w \propto \omega \langle p \rangle V_{SW} / (RT) \tag{7.5}$$

Thus from (7.4) and (7.5),

$$\Delta T / T \propto \dot{Q}\{(\gamma - 1)/(\langle p \rangle \gamma)\}/(\omega V_{SW}) \tag{7.6}$$

From Table 3.2, for large unswept volumes, fixed temperatures and volume phase angles close to 90° the work may be shown to be proportional as follows:

$$W \propto \langle p \rangle V_{SW}^2 / V_D \tag{7.7}$$

where the swept volumes are assumed to be of similar order.

In terms of power, (7.7) becomes

$$P \propto \omega \langle p \rangle V_{SW}^2 / V_D \qquad (7.8)$$

From (7.6) and (7.8)

$$\Delta T / T \propto \dot{Q}[(\gamma - 1)/\gamma][\omega \langle p \rangle P V_D]^{-1/2} \qquad (7.9)$$

Heat exchangers with similar ΔT will have similar ΔT irreversibility. Thus comparing engines charged with hydrogen and helium to air with identical Q, P, ω, $\langle p \rangle$ and V_D, we have:

$$(\Delta T / T)_{H2} / (\Delta T / T)_{air} = 1.01 \qquad (7.10)$$

$$(\Delta T / T)_{He} / (\Delta T / T)_{air} = 1.40 \qquad (7.11)$$

which suggests that air has lower axial ΔT irreversibility which is expected since it has the higher heat capacity at similar pressure. It will be shown that engines optimised for air charging lead to higher pressures and larger dead volumes compared to hydrogen or helium charged engines, particularly at higher power levels. Thus from (7.9) it can be seen that the axial ΔT irreversibility is an even bigger advantage for air in such cases.

Heat transfer per unit viscous dissipation is also a useful measure to compare the performance of different working gases. From §4.4, Equations (4.44) and (4.52), the heat transfer per unit viscous dissipation for both laminar and turbulent flow is proportional as follows:

$$\langle \dot{Q} \rangle / \langle \Phi \rangle \propto \left[(k \, \Delta T_{wg}) / (\mu \omega^2 V_{sw}^{\;2}) \right] (A_h n)^2 \qquad (7.12)$$

From (7.8) and (7.12) and assuming (for the sake of simplicity) that the dead volume is proportional to the flow area, the following is obtained:

$$\langle p \rangle A \;\propto\; \mu \omega P / (k \, \Delta T_{wg}) \left[\langle \dot{Q} \rangle / \langle \Phi \rangle \right] \qquad (7.13)$$

where A is the total free flow area.

Therefore, for similar $\langle \dot{Q} \rangle / \langle \Phi \rangle$, P, ΔT_{wg} and ω, the following ratios are obtained:

$$\left[\langle p \rangle A \right]_{H2} / \left[\langle p \rangle A \right]_{air} = 0.070 \text{ at 300K and } 0.067 \text{ at 1000K} \qquad (7.14)$$

$$\left[\langle p \rangle A \right]_{He} / \left[\langle p \rangle A \right]_{air} = 0.198 \text{ at 300K and } 0.305 \text{ at 1000K} \qquad (7.15)$$

$$\left[\langle p \rangle A \right]_{H2} / \left[\langle p \rangle A \right]_{He} = 0.354 \text{ at 300K and } 0.22 \text{ at 1000K.} \qquad (7.16)$$

which indicates that the product of charge pressure and flow area for air engines is much greater than that for equivalently performing hydrogen or helium engines. This suggests that an equivalently performing air engine will either be pressurized to a higher degree or the flow area will be greater or both higher pressure and larger flow area. The hydrogen engine offers the best opportunity for lowest pressure and smallest flow area.

Again from (7.8) and (7.12), assuming dead volume to be directly proportional to the flow area and eliminating the flow area between the equations, the product of swept volume and pressure scale according to:

$$V_{sw}\langle p\rangle \propto [\mu/(k\,\Delta T_{wg})]^{1/2}[\langle \dot{Q}\rangle/\langle\Phi\rangle]^{1/2}p \qquad (7.17)$$

which leads to

$$[V_{sw}\langle p\rangle]_{H2}/[V_{sw}\langle p\rangle]_{air} = 0.265 \text{ at 300K and } 0.259 \text{ at 1000K} \qquad (7.18)$$

$$[V_{sw}\langle p\rangle]_{He}/[V_{sw}\langle p\rangle]_{air} = 0.445 \text{ at 300K and } 0.552 \text{ at 1000K} \qquad (7.19)$$

$$[V_{sw}\langle p\rangle]_{H2}/[V_{sw}\langle p\rangle]_{He} = 0.595 \text{ at 300K and } 0.469 \text{ at 1000K.} \qquad (7.20)$$

which again shows that the equivalently performing air engine will have a much larger swept volume and/or pressure than either a helium or hydrogen engine.

It is instructive to compare engines of identical performance and charge pressure. To do this it will be be assumed that the swept volume cross sectional area is equal to the flow area for the engine with smallest flow area and that the engines have identical strokes. Thus from (7.14) through (7.16) and (7.18) through (7.20), the total engine areas would scale as follows:

$$[A_{engine}]_{H2} / [A_{engine}]_{air} \approx 0.11 \tag{7.21}$$

$$[A_{engine}]_{He} / [A_{engine}]_{air} \approx 0.33 \tag{7.22}$$

$$[A_{engine}]_{H2} / [A_{engine}]_{He} \approx 0.36 \tag{7.23}$$

Thus an equivalently performing air engine of similar power may be some nine times greater than the total cross sectional area of a hydrogen engine and three times the cross sectional area of a helium engine. This is some three times larger on diameter than the hydrogen engine and just under twice the diameter of the helium engine. The helium engine diameter is about 1.7 times the diameter of, an equivalently performing hydrogen engine for these conditions.

There are a few provisions that must be made concerning the above results. The first is that flow induced compressibility is not considered. The limiting engine speed for a hydrogen engine is much higher than either a helium or an air engine partly due to the lower viscosity and density but also due to a significantly higher sonic velocity. At the onset of significant flow induced compressibility, the simple working gas comparisons are likely to break down. The second provision is that for the working gas comparisons to hold, the engines must perform equivalently. It is not indicated to what degree the performance will differ with different working gases for engines not performing identically. The difference may be marginal or significant. For example, if a helium engine had very high NTU heat exchangers as shown in Figure 7.3, it is clear that

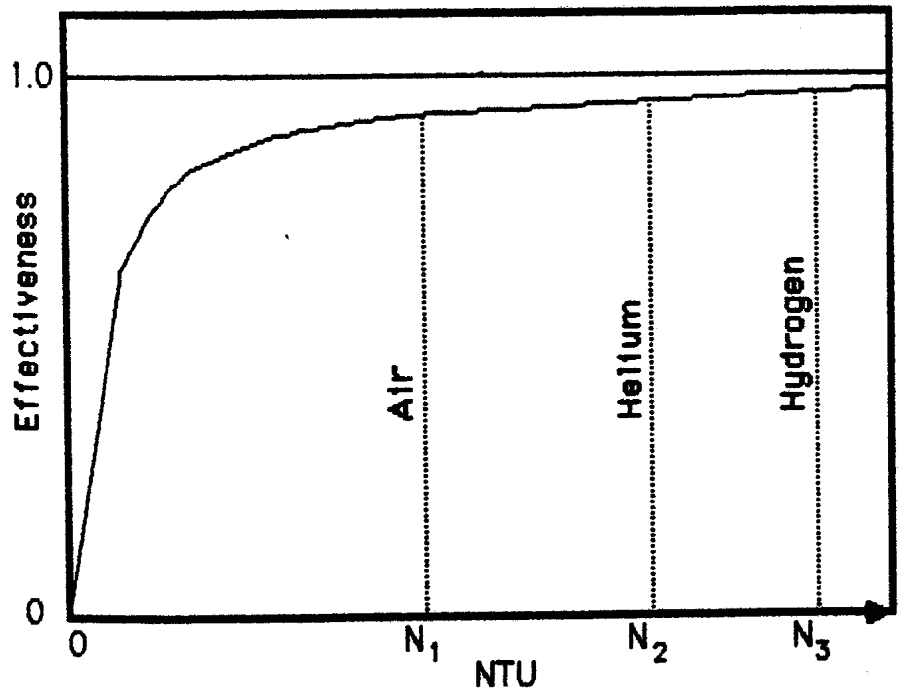

Figure 7.3 The Effect of Different Working Gases on a High NTU Heat Exchanger

(The effectiveness - NTU relationship is not a function of gas properties for fixed heat capacity ratio [Ho76])

the effectiveness of the heat exchangers would be almost constant over a large range of NTU. Replacing the working gas with air in this situation will reduce the NTU due to the lower heat transfer coefficient, but not necessarily to a point where the effectiveness suffers significantly. Charging with hydrogen would increase the NTU of an already effective heat exchanger and therefore also not make much difference. The heat capacity ratio $(c_p w)_{min} / (c_p w)_{max}$ could be maintained constant by adjusting the mass flow of the external heat transfer fluid and so need not be considered in this argument (see Holman [Ho76] pp403-405). Various workers (Meijer [Me70], Urieli [Ur77], Berchowitz *et al* [BU79]) have noticed that at low speeds a Stirling engine charged with air could have about the same performance as when charged with helium or hydrogen (in some cases the performance with air may even be better [Ur77]). Since the heat exchangers are generally designed to operate at higher frequencies with helium or hydrogen, the NTU at low speeds would be much higher thus reducing the performance difference between the various gases. Figure 7.4 is taken from Meijer's work and clearly shows the performance difference of the various gases closing at lower engine speeds and, at the high speed point where the performance of the lighter gases begins to drop off, the disadvantage of air is greatest. Urieli [Ur77] noticed that the peak powers for air, helium and hydrogen for an arbitrary engine appear to be in the proportion of their sonic velocities. This may be indicative of flow induced compressibilities being the limiting factor for maximum power.

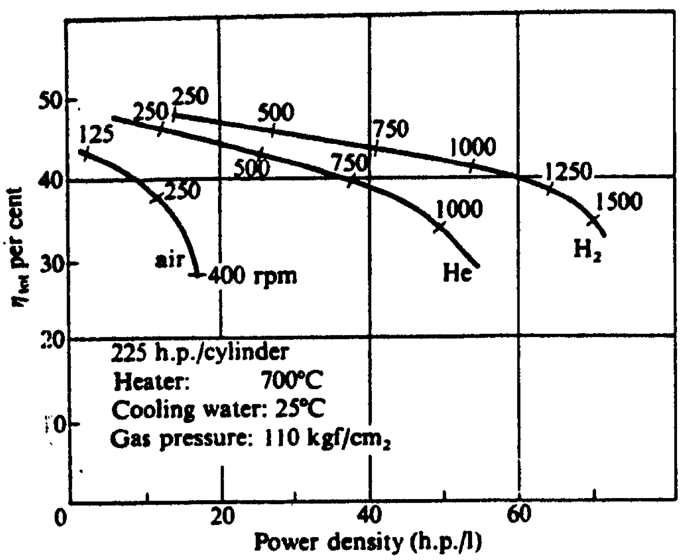

Figure 7.4 Performance Curves for Different Working Gases [Me70]

No mention has been made of the other irreversibilities that are affected by choice of working gas. In S6.3 it was shown that air exhibits lowest hysteresis losses with hydrogen being slightly worse. Helium has the highest hysteresis loss of the gases considered here. Gas conduction losses would of course also favour air. A comparison of performance of geometrically identical air and helium charged engines is given in Table 7.1. It can be seen that in order to obtain comparable power, the pressure of the air engine is higher as would be expected. In this particular engine the gas flow areas are large and the heat exchangers have high NTU.

Table 7.1 Loss Inventory of Helium and Air Engines of Identical Size (Data obtained from computer simulation [BR85])

	Air	Helium
Power [kW]	4.57	4.63
Efficiency [%]	29.1	33.9
Pressure [bar]	23.0	19.0
Frequency [Hz]	60.0	60.0
Leakage Loss [W]	269.0	236.0
Gas Spring Loss [W]	89.3	365.0
Cooler Pumping [W]	117.0	37.0
Heater Pumping [W]	502.0	324.0
Regenerator Pumping [W]	1146.0	618.0
Regen. Enthalpy Loss [W]	3119.0	1097.0
Displacer Conduction [W]	44.1	142.0
Regen. Gas Cond. [W]	28.9	84.8
Appendix Gap Loss [W]	255.0	196.0
Wall conduction [W]	201.0	166.0

Working gas hysteresis losses are accounted for in the simulation at a basic level and are therefore not listed here. These losses reduce the mechanical work and alter the heat transfer. Note also that pumping losses referred to here are the viscous dissipation losses.

A general conclusion that may be drawn from this section is that air, helium and hydrogen engines can perform to similar powers and efficiencies but air and helium engines will have significantly poorer specific power with air being the poorest. Furthermore, an equivalently performing air engine will have much more extensive heat exchangers than either the helium or hydrogen charged engines. However, at the lower powers or situations where specific power (or power density) is not of particular importance, air may be the better choice due to its appreciable practical advantages in sealing, replenishment and simple engine design.

7.3 Selection of Charge Pressure

Since ideal power is directly proportional to charge pressure (Table 3.2), Stirling engines are generally pressurized to improve their power density (kW/m^3). However, there are two limiting factors to pressurizing to high levels, *viz*, as the power density is increased, the available area for external heat transfer is reduced and secondly, since leakage losses are proportional to the square of the pressure (Table 6.1), the effect of leakage becomes dominant at high pressure. All other parasitic losses are either directly proportional to, or less than directly proportional to pressure. Thus if leakage loss was neglected, the power would essentially be directly proportional to pressure until the point where transferring the external heat across the available area becomes impractical.

The SPIKE engine, a 5.5kW low technology air engine [WC82] and a recent 3kW free-piston air engine [BR85] are all relatively low pressure engines and therefore have characteristically large diameters. Low pressure engines tend to have favourable surface area geometry for integrally finned heat exchangers that can be easily manufactured by investment casting. The heat flux limit varies with the design of the heat source (and sink), typical heat fluxes for a gas combustor range anywhere between $100 kW/m^2$ to $400 kW/m^2$. The higher value corresponds to higher blower powers and/or temperatures and smaller heat transfer area.

The following illustrates the effect of some design parameters on heat flux for an integrally finned head.

From the definition of engine efficiency, the heat transfer to the engine may be written

$$\dot{Q} \propto P/\eta \tag{7.24}$$

The heat transfer surface area is proportional to engine diameter and stroke (a longer heat exchanger is generally required for a longer stroke), thus for fixed power the heat flux becomes

$$(\dot{Q}/A_W) \propto P/(\eta D X_p) \tag{7.25}$$

Rewriting the simple power proportion (7.8)

$$P \propto \omega \langle p \rangle V_{SW}^2 / V_D \tag{7.8}$$

(repeated)

Assuming that dead volume is approximately proportional to the swept volume, (7.8) becomes

$$P \propto \omega \langle p \rangle V_{sw} \tag{7.26}$$

This approximate relationship was first identified by Beale and has been mentioned many times in the literature [Wa80], [We81] and [WS85], the constant of proportionality has become known as the Beale number (Be).

Writing swept volume in terms of diameter and stroke, (7.26) becomes

$$P \propto \omega \langle p \rangle D^2 X_p \tag{7.27}$$

Making the diameter the subject of (7.27) and substituting into (7.25) gives

$$(\dot{Q} / A_w) \propto (1/\eta)\sqrt{P\omega\langle p \rangle / X_p} \tag{7.28}$$

Thus for engines of similar power and efficiency, the heat flux increases as the square root of frequency and pressure and to the square root of the inverse stroke. A low technology air charged engine would therefore be expected to have long stroke, low frequency and low pressure as was indicated by Wood *et al* [WC82].

As has been mentioned, the other limitation to high charge pressures is the effect of internal leakage losses.

From Table 6.1, writing the seal leakage loss for a piston clearance seal,